Elastic wavefield extrapolation in HTI media

Richard A. Bale and Gary F. Margrave

ABSTRACT

A wavefield extrapolation operator for elastic anisotropic media can be constructed from solutions of the one-way elastic-wave equation, solutions which are related to those of the Kelvin-Christoffel equation. Aside from an initial decomposition, which depends upon boundary conditions, the extrapolation is simply described by two matrix operations. The first, a diagonal matrix, applies the phase shift for each of the three elastic modes, P, S1 and S2. The second, a 3-by-3 "interface-propagator" matrix, describes the effects of crossing depth interfaces with changes in medium properties. These are sub-matrices of the general propagator matrices, conventionally used for two-way wavefield propagation. The interface-propagator matrix includes all forward-scattered mode-conversions in its full form. It can be modified in the extrapolation algorithm to select only those conversions of interest. In particular we consider the selection of only those conversions between shear-wave modes S1 and S2 which describe the onset of HTI type anisotropy. The result is an extrapolator which performs the equivalent of an Alford rotation valid at all angles of propagation. We consider two possible boundary conditions, one corresponding to a stress-free surface, and the other an infinite half-space.

INTRODUCTION

Wavefield extrapolation is at the heart of the class of migration algorithms commonly referred to as *wave equation* migration. A wavefield extrapolator, as used in such migration schemes, generates the wavefield at depth $z+\Delta z$ from the wavefield at depth z, given the medium parameters over the depth interval. This is usually done over small enough depth intervals that the medium may be approximated as invariant with respect to z over each interval.

In the derivation of a wavefield extrapolator, an important concept is that of a one-way wave equation. Use of a one-way wave equation avoids some of the complexity associated with multiple scattering, is more robust to velocity errors, and is in general more computationally efficient than methods based on the full two-way wave equation. In the case where the medium parameters depend only upon depth (and are constant over each depth interval), and where a scalar wave equation is assumed, the one-way wave equation can be derived by a simple factorization of the two-way wave equation in the frequency-wavenumber domain, giving rise to a phase-shift algorithm (Gazdag, 1978).

In more realistic cases where the medium varies laterally, a standard approach is to assume a solution of the same form, but where the velocity parameter is now a function of lateral position. This gives rise to extrapolators which may be framed within pseudodifferential operator theory. One such form is a limiting case of the popular phase shift plus interpolation (PSPI) algorithm of Gazdag and Sguazzero (1984). An alternative algorithm can be derived from the corresponding adjoint form of the pseudodifferential operator and is known as nonstationary phase shift (NSPS), having arisen from the theory

of nonstationary filtering (Margrave and Ferguson, 1999). The two approaches have somewhat differing properties, and can give visibly different results for large depth steps, though their behaviour converges as the depth step shrinks. In practice, efficiency demands that the full pseudodifferential operators of PSPI or NSPS are approximated using a set of spatially invariant reference operators and an interpolation scheme, in order to allow use of the fast Fourier transform. A new method known as adaptive Gabor phase-shift (AGPS), which aims to optimize this interpolation based on the spatial variation of the model, is currently being investigated (Grossman et al., 2002a, 2002b).

The above remarks are primarily based on research into scalar-wave equation extrapolators. These are strictly only appropriate for migration in acoustic media, though they have been highly successful when applied to the migration of P-wave data acquired in conventional seismic surveys. Nevertheless, there are some disadvantages in using a scalar-wave equation when it comes to extrapolation of elastic-wave data, as are acquired in multicomponent surveys. First of all, the scalar-wave approach assumes that each wave-mode (such as P, SV and SH for the isotropic case) can be handled independently of the others, after appropriate wavefield decomposition. In fact conversion between modes is commonplace. Secondly, scalar wavefield extrapolation is unable to keep track of changes in polarization, especially important for shear-waves, which occur during wave propagation. This places an undesirable limitation on how accurately amplitudes can be recovered. Finally, it is difficult to account fully for effects of anisotropy, such as shear-wave splitting, using a scalar extrapolator. For these reasons it is desirable to approach elastic wavefield extrapolation from a *vector* (or, more accurately, *tensor*) wave equation standpoint. It will transpire that *locally* (within each depth step) the extrapolation may be transformed into three scalar extrapolations, in combination with a mode conversion operator.

For another perspective on anisotropic elastic extrapolation, consider processing of shear-wave data in the presence of shear-wave splitting, as occurs in surveys over fractured reservoirs. Currently the standard approach is to apply Alford rotation (Alford, 1986) or one of a host of related methods (Gaiser, 2000; Bale et al., 2000). The assumption underlying all of these methods is that the isolation of the fast (S1) and slow (S2) shear waves can be achieved by rotation of the horizontal components to principal axes using a standard rotation matrix. A shift correction can then be applied to compensate for phase differences between the two modes so that they may be coherently combined. Assuming the medium in question is transversely isotropic with a horizontal axis of symmetry (HTI), this approach is valid for shear-wave energy propagating vertically or near vertically, assuming low relief structure. The theoretical basis breaks down in the presence of large source-receiver offset or significant structural dip. It can be easily shown that the diagonalization and shifting operations of Alford rotation are recovered from the HTI elastic wavefield extrapolators described here, by setting the wavenumber to zero. However, the elastic extrapolators are not limited by dip or offset assumptions. So from this perspective, HTI elastic extrapolation could be regarded as all-offset all-dip Alford rotation.

The theory of elastic wavefield extrapolation is well established. Wapenaar and Berkhout (1989) give a comprehensive exposition of this theory using both two-way and

one-way wave equations, for the case of isotropic media. Zhe and Greenhalgh (1997) proposed a migration algorithm for elastic waves in isotropic media. Their extrapolation step consists of decomposing the displacement into potentials via the Helmholtz decomposition, extrapolating the potentials using a split-step technique (Stoffa et al., 1990), and then recomposing to displacement. Their method uses a finite-difference wavefield decomposition, which requires knowledge of the wavefield at a few adjacent depth intervals in order to compute the vertical derivative. The depth steps are initialized below the surface by applying a few steps of reverse time migration. Etgen (1988) instead performed wavefield separation in the wavenumber domain using Fourier transformed divergence and curl operators, applied to the displacement data, before scalar migration of P and SV potentials with a Stolt algorithm. Hou and Marfurt (2003) sidestep the decomposition problem by extrapolating each component of displacement using scalar extrapolators, and applying the separation step as part of the imaging condition. They found that doing so enabled a PS separation which is less sensitive to model errors. A possible disadvantage, particularly for anisotropic media, is the need to extrapolate each of 3 components using 3 different models. As shown by Dellinger and Etgen (1990), the Helmholtz decomposition for elastic waves can be generalized to anisotropic media by using the Christoffel equation. In our algorithm we apply this decomposition at each depth step and extrapolate the different wave-modes using anisotropic slownesses. By working in the spatial Fourier domain, where the vertical slowness is implicitly determined from horizontal slowness, and by assuming one-way propagation, we avoid the need to combine multiple depth steps in the wavefield decomposition. A stress-free boundary condition can be used as an alternative to assuming one-way wave propagation at the surface.

The structure of this paper is as follows. We review the theory of elastic-wave propagation, deriving eigensolutions to the Kelvin-Christoffel equation using the Stroh formalism from mechanics (Ting, 1996; Shuvalov, 2001). These provide both the required vertical slownesses and the polarization vectors needed for extrapolation. We then derive the appropriate one-way operators, leaning heavily on the work of Fryer and Frazer (1984, 1987), which in turn is based on Kennett's (1983) work. We show that the operator which extrapolates the three elastic modes can be described by a combination of a diagonal matrix containing phase shifts for each mode and an "interface-propagator" matrix which includes terms describing mode conversions. As applied to forward modeling by Silawongsawat (1998), the terms of the interface-propagator can be used selectively, for example, to omit conversion between P and S, but include conversion between S1 and S2 modes arising from a change in the principal axes orientation. Examples are shown to illustrate the operators for both isotropic and HTI media. The extension to laterally varying media, via PSPI and NSPS type algorithms, is discussed in a companion paper (Bale and Margrave, 2003).

THEORY

Consider an acoustic wavefield $\phi(x, y, z, t)$, in a homogeneous medium with velocity c. The scalar-wave equation, after Fourier transforming over time and the lateral spatial variables x and y, is

$$\frac{\partial^2 \tilde{\phi}}{\partial z^2} + \omega^2 \left(\frac{1}{c^2} - \left(s_x^2 + s_y^2 \right) \right) \tilde{\phi} = 0 , \tag{1}$$

where $\tilde{\phi}\left(s_x, s_y, z, \omega\right)$ is the Fourier-transformed wavefield, defined by

$$\tilde{\phi}\left(s_x, s_y, z, \omega\right) = \int_{-\infty}^{\infty} \int_{-\infty}^{\infty} \int_{-\infty}^{\infty} e^{i\omega\left(s_x x + s_x x - t\right)} \phi\left(x, y, z, t\right) dx dy dt ,$$

The Fourier variables used here and subsequently are the wave slownesses in *x* and *y* directions, s_x and s_y, and the angular frequency ω.

An important feature of equation (1) is the isolation of the main propagation direction, taken here to be the vertical direction, *z*. Doing so enables analysis in terms of one-way solutions which are either upward or downward propagating. By selecting only the down-going solution, the wavefield may be extrapolated in a way which neglects unwanted backward scattering. The one-way extrapolator which satisfies (1) is

$$\tilde{\phi}\left(s_x, s_y, z, \omega\right) = \exp\left(i\omega s_z \left(z - z_0\right)\right) \tilde{\phi}\left(s_x, s_y, z_0, \omega\right), \tag{2}$$

where $s_z = \sqrt{1/c^2 - \left(s_x^2 + s_y^2\right)}$ is the vertical slowness. That (2) is a solution to (1) can be verified by direct substitution.

We now turn our attention to elastic, vector wavefields.

Eigensolutions to elastic-wave equation

The constitutive and momentum equations governing elastic-wave propagation are

$$\sigma_{ij} = c_{ijkl} u_{k,l} \tag{3a}$$

$$\rho \ddot{u}_i = \sigma_{ij,j} + f_i \tag{3b}$$

Here u_i refers to the i[th] component of the particle displacement vector **u**, ρ is the medium density, c_{ijkl} is the stiffness tensor, and f_j is the body force. We use the convention that "$,j$" denotes partial differentiation with respect to x_j, the j[th] spatial coordinate, and the Einstein summation convention for twice-repeated indices. Indices take the values 1, 2 and 3, with $x_1 \equiv x$, $x_2 \equiv y$ and $x_3 \equiv z$.

Combining equations 3, and neglecting body forces, gives the elastic-wave equation

$$\rho \ddot{u}_i = c_{ijkl} u_{k,jl} . \tag{4}$$

Substitution of plane-wave trial solutions of the form $\mathbf{u} = U e^{i\omega\left(\mathbf{s}\cdot\mathbf{x} - t\right)} \mathbf{p}$, where $\mathbf{p} = \left(p_1 \;\; p_2 \;\; p_3\right)^T$ and $\mathbf{s} = \left(s_1 \;\; s_2 \;\; s_3\right)^T$ are the polarization and slowness directions

respectively, into (4), gives the Kelvin-Christoffel equation (e.g. Musgrave, 1970), which can be written in either of two forms:

$$\left(\Gamma^{0}_{ik} - v^2 \rho \delta_{ik}\right) p_k = 0 \tag{5a}$$

$$\left(\Gamma_{ik}(\mathbf{s}) - \rho \delta_{ik}\right) p_k = 0\,, \tag{5b}$$

where $\Gamma^0_{ik} = c_{ijkl}\hat{n}_j\hat{n}_l$ and $\Gamma_{ik}(\mathbf{s}) = c_{ijkl}s_j s_l$ are the two forms of the Christoffel matrix, $\hat{\mathbf{n}} = v\mathbf{s}$ is the unit vector in the slowness direction, with v being the wavespeed, and δ_{ik} is the Krönecker delta function.

The first form, (5a), gives rise to a true eigenvalue problem, in which the eigenvalues are $v^2\rho$. There are in general three such values corresponding to qP (quasi-P), qS1 (quasi-S1) and qS2 (quasi-S2) modes. Since $\mathbf{\Gamma}^0$ is real, symmetric and positive definite, for real $\hat{\mathbf{n}}$ (Musgrave, 1970), all eigenvalues are real and positive, giving real wavespeeds, which can be chosen positive. The normalized eigenvectors are the polarizations $\mathbf{p}$, which are orthogonal for a given $\hat{\mathbf{n}}$.

The second form, (5b), is more convenient for wavefield extrapolation, since we may fix the radial (horizontal) slowness $\mathbf{s}_r = (s_x, s_y) \equiv (s_1, s_2)$, and solve for the vertical slowness $s_z \equiv s_3$. In this alternative problem, the "eigenvalues" (a misuse of the term, but common in the literature) are the values of s_z. The characteristic equation $\det\left(\Gamma_{jl} - \rho\delta_{jl}\right) = 0$ has 6 roots for s_z. For non-evanescent waves (real s_z), the matrix $\mathbf{\Gamma}$ is real and symmetric. However, it is *not* the case that the resulting "eigenvectors" (again, a misuse) are orthogonal. For example, if we consider the qP, qS1 and qS2 waves associated with a given radial slowness, $\mathbf{s}_r$, (but different vertical slownesses), they correspond to three different slowness directions, $\hat{\mathbf{n}}$, and have non-orthogonal polarizations. This is illustrated in Figure 1.

In general, the sixth-degree equation implied by (5b) has no analytic solution, and must be solved numerically. Fortunately, for anisotropy of sufficient symmetry, (5b) is cubic in s_z^2, and may be analytically solved (Fryer and Frazer, 1987). In the HTI case, as in the VTI case, the solution for s_z^2 splits into a quadratic and a linear term, making solution quite straightforward. The solutions form pairs $\pm s_z$, which correspond to up- and down-going waves. The three pairs of vertical slownesses correspond to different wave-modes $s_z^{(P)}$, $s_z^{(S1)}$ and $s_z^{(S2)}$, and have corresponding polarization vectors $\mathbf{p}^{(P)}$, $\mathbf{p}^{(S1)}$ and $\mathbf{p}^{(S2)}$. For HTI the polarizations of up- and down-going waves are simply related by changing the sign of the z component and leaving the horizontal components unchanged. For a generic mode, these are indicated by $s_z^{(M)}$ and $\mathbf{p}^{(M)}$, where $M \in \{P, S1, S2\}$, dropping the preceding qualifier, "q", for brevity.

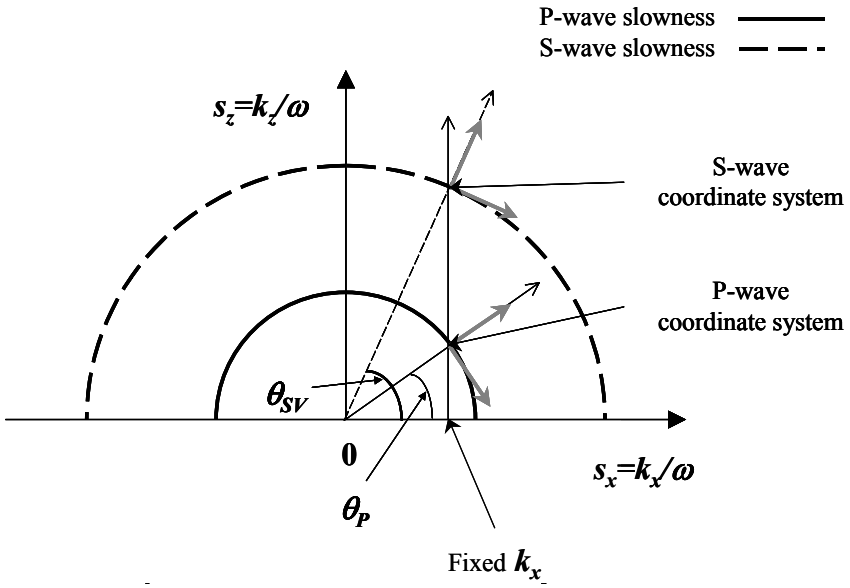

FIG 1. P-wave and S-wave phase velocities (bold and dashed curves). Phase angles θ_P and θ_{SV} (isotropic case) for a given horizontal slowness, s_x, corresponding to fixing k_x for a given frequency ω., as required for wavefield extrapolation. For any given phase angle there is a unique orthonormal set of basis vectors given by the polarizations of P, S1 and S2 modes, defining a coordinate system in which propagation is (locally) decoupled. For any given k_x the polarizations of the different modes are not orthogonal.

The wavespeed, v_M, is given by $1/v_M^2 = \mathbf{s}_r \cdot \mathbf{s}_r + \left(s_z^{(M)}\right)^2$. In general v_M is a function of the slowness (phase) direction. For the isotropic case, v_M is constant and we can solve for vertical slowness easily via $s_z^{(M)} = \pm\sqrt{v_M^{-2} - s_r^2}$. For $s_r^2 \le 1/v_M^2$ solutions are real, but for $s_r^2 > 1/v_M^2$ they are imaginary, corresponding to evanescent waves. This gives rise to three distinct regions: (I) $|s_r| < 1/v_P < 1/v_S$ leading to real s_z for all modes; (II) $1/v_P < |s_r| < 1/v_S$ leading to real $s_z^{(SV,SH)}$ but imaginary $s_z^{(P)}$; and (III) $1/v_P < 1/v_S < |s_r|$ for which all s_z are imaginary. Likewise, for anisotropy, complex values for s_z can arise when the Christoffel equation is solved. There are four such regions, since the S-wave wavespeeds differ, creating an additional region between $1/v_{S1}$ and $1/v_{S2}$. Figure 2 shows the variation of vertical slowness for each mode as a function of horizontal slowness for isotropic and HTI cases. Since the HTI case is taken to be in the plane containing the axis of symmetry, the two shear modes decouple. The S1 mode can be regarded as SH and the S2 mode as SV.

Determination of the polarization vectors is not completely trivial. A solution to equation (5b) is of the form (Shuvalov, 2001)

$$\mathbf{p} = \mathrm{adj}\left(\mathbf{\Gamma}(\mathbf{s}) - \rho\mathbf{I}\right)\mathbf{w} \ , \qquad (6)$$

where **w** is an arbitrary vector, **I** is the identity matrix (i.e. matrix form of Krönecker delta), and adj(**A**) means the adjugate of **A**, obtained by replacing each element of **A** by its signed cofactor, and transposing, as follows:

$$\text{adj}(\mathbf{A}) = \begin{pmatrix} C_{11} & C_{21} & C_{31} \\ C_{12} & C_{22} & C_{32} \\ C_{13} & C_{23} & C_{33} \end{pmatrix},$$

where the cofactors of **A** are: $C_{11} = \det\begin{pmatrix} a_{22} & a_{23} \\ a_{32} & a_{33} \end{pmatrix}, C_{12} = -\det\begin{pmatrix} a_{12} & a_{13} \\ a_{32} & a_{33} \end{pmatrix}$, etc.

The definition of adjugate is constructed so that $\mathbf{A}\,\text{adj}(\mathbf{A}) = \det(\mathbf{A})\mathbf{I}$, and, when the determinant is non-zero, the inverse of **A** exists and is given by $\mathbf{A}^{-1} = \text{adj}(\mathbf{A})/\det(\mathbf{A})$. That equation (6) solves equation (5b) follows directly from the fact that $\det(\mathbf{\Gamma}(\mathbf{s}) - \rho\mathbf{I}) = 0$. However, simple substitution of the three eigenvalues, $s_z^{(P)}$, $s_z^{(S1)}$ and $s_z^{(S2)}$, into equation (6) does not necessarily lead to distinct eigenvectors, unless **w** is also changed, due to the presence of degenerate solutions and/or null rows in the adjugate matrix. Fryer and Frazer (1987) provide a solution, which corresponds to choosing $\mathbf{w} = (0 \quad 0 \quad 1)^T$ for P-waves, and then trying $\mathbf{w} = (0 \quad 1 \quad 0)^T$ and $\mathbf{w} = (1 \quad 0 \quad 0)^T$ for each S-wave mode in turn. While this gives linearly independent solutions for most cases, an unfortunate counter-example is the isotropic case, for which the adjugate matrix is identically zero. Nonetheless, polarizations are easily determined for the isotropic case, with the usual choice of S-waves corresponding to SV and SH, giving the polarizations as

$$\mathbf{p}^{(P)} = \begin{pmatrix} v_P s_x \\ 0 \\ v_P s_z^{(P)} \end{pmatrix}, \quad \mathbf{p}^{(SH)} = \begin{pmatrix} 0 \\ 1 \\ 0 \end{pmatrix}, \quad \mathbf{p}^{(SV)} = sign(s_x) \begin{pmatrix} -v_S s_z^{(SV)} \\ 0 \\ v_S s_x \end{pmatrix}. \qquad (7)$$

In (7) the vectors have complex-valued elements for some wavenumbers, and can be written in the form, $\mathbf{p} = \mathbf{p}_R + i\mathbf{p}_I$, known as *bivectors* (Shuvalov, 2001). Using the same classification as for the vertical slownesses we find the following behaviour, for the isotropic case: in (I) all elements of the polarizations are real; in (II) all elements are real except $p_3^{(P)}$, which is imaginary; in (III) all elements are real, except for $p_3^{(P)}$ and $p_1^{(SV)}$. Figure 3 shows the real and imaginary components of $\mathbf{p}^{(P)}$ and $\mathbf{p}^{(SV)}$ for an isotropic medium, as a function of horizontal slowness, s_x. The second elements are omitted, as they are zero. Of particular interest are the complex elements that arise in the zone between P- and S-wave evanescent cutoffs. In equation (7) and Figure 3, a polarity convention has been adopted such that both P and SV amplitudes are symmetric about normal incidence. Since the horizontal displacement is an antisymmetric function, this forces an antisymmetric behaviour on the X-component of both polarizations. We also use the convention that the X-component of polarizations should be positive for $s_x > 0$, and show the case for an upward-propagating wave, such that $s_z < 0$.

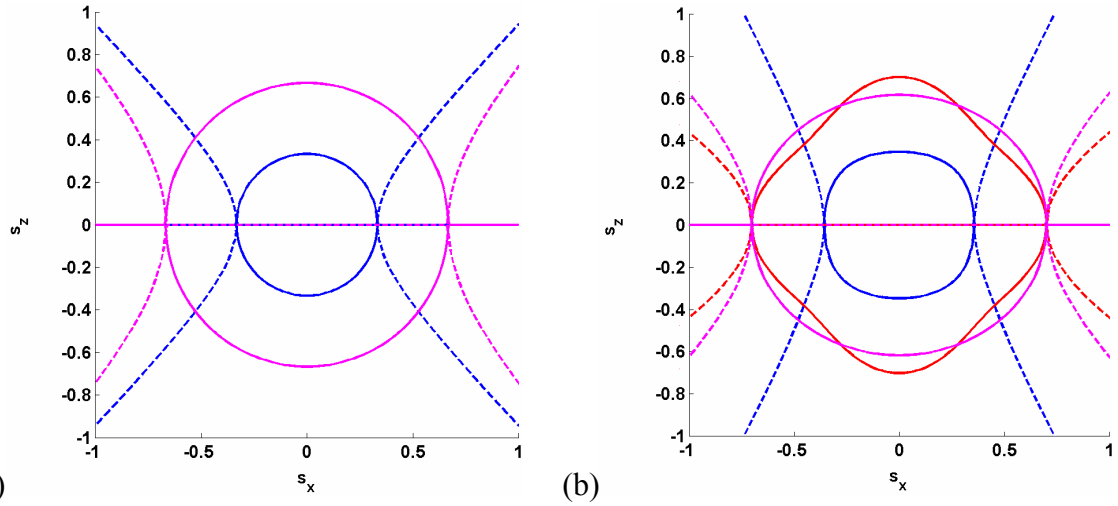

FIG. 2. Vertical slowness against horizontal slowness for: (a) an isotropic medium, with v_P=3000m/s, v_S=1500m/s. and; (b) an HTI medium, along plane containing symmetry axis. Plots show real (solid) and imaginary (dashed) values for P-waves (blue), SV-waves (red) and SH-waves (magenta). In the isotropic case, the SV and SH curves are coincident.

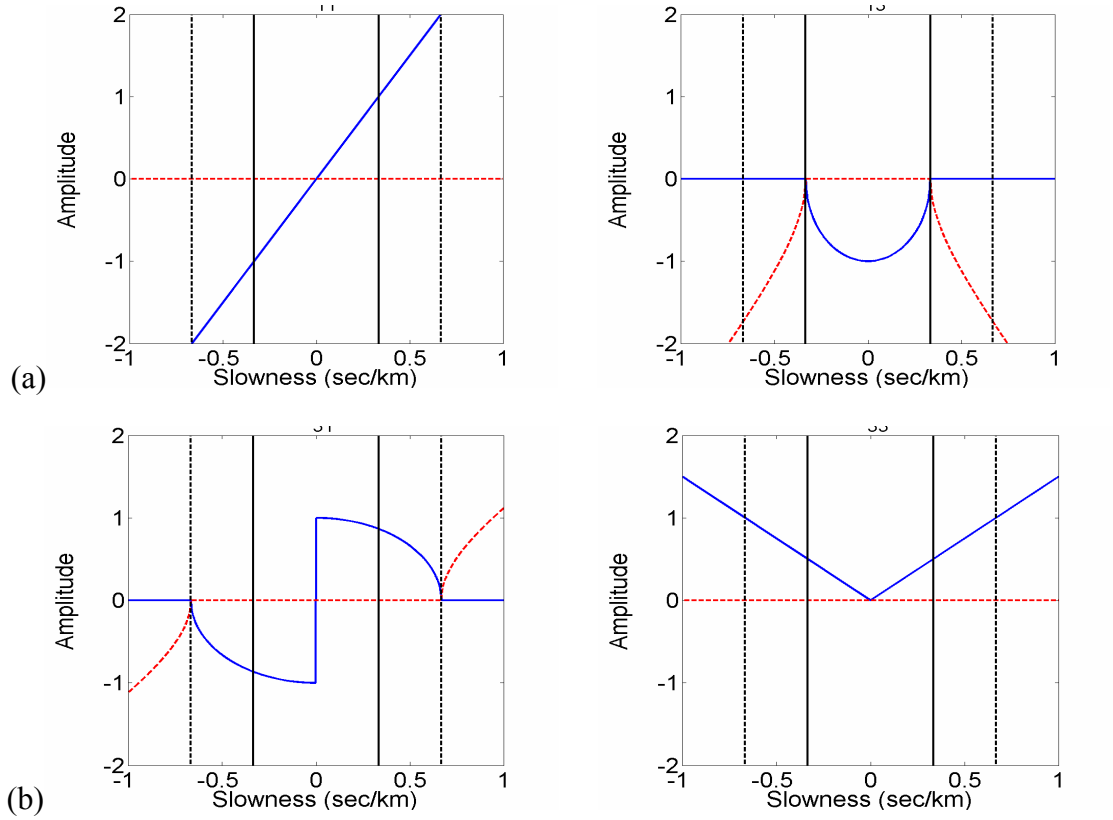

FIG. 3: (a) P-wave polarization as a function of horizontal slowness, for an up-going wave in an isotropic medium with v_P=3000m/s, v_S=1500m/s. The X (left) and Z (right) components are shown. Real parts are blue solid, imaginary parts are red dashed. The vertical lines show the evanescent cut-off boundaries for P-waves (solid lines) and for S-waves (dashed lines). (b) SV-wave polarization for the same medium, X-(left) and Z-(right) components.

Two-way equation

We now seek a vector equation for elastic-wave propagation which is analogous to equation (1). We Fourier transform (4) with respect to *x*, *y* and *t*, to obtain

$$T_{ik}u_{k,33} - i\omega\left(R_{ik}+R_{ki}\right)u_{k,3} - \omega^2 Q_{ik}u_k + \rho\omega^2 u_i = 0\,, \tag{8a}$$

where $u_i\left(\mathbf{s}_r, z, \omega\right)$ is the Fourier transform of $u_i\left((x,y),z,t\right)$, and the 3-by-3 matrices, **Q**, **R** and **T**, are given by (e.g. Ting, 1996; Shuvalov, 2001)

$$\begin{aligned} Q_{ik} &\equiv c_{i1k1}s_1^2 + \left(c_{i1k2}+c_{i2k1}\right)s_1 s_2 + c_{i2k2}s_2^2 \\ R_{ik} &\equiv c_{i1k3}s_1 + c_{i2k3}s_2 \\ T_{ik} &\equiv c_{i3k3} \end{aligned}\,. \tag{8b}$$

In matrix notation, equation (8) is written

$$\mathbf{T}\frac{\partial^2\mathbf{u}}{\partial z^2} - i\omega\left(\mathbf{R}+\mathbf{R}^T\right)\frac{\partial\mathbf{u}}{\partial z} - \omega^2\left(\mathbf{Q}-\rho\mathbf{I}\right)\mathbf{u} = 0\,. \tag{9}$$

Equation (9) is a second-order differential vector equation which is analogous to the second-order differential scalar equation (1). As in the scalar case, the vertical direction is isolated from the other two spatial directions by the Fourier transform.

It is reassuring to see that equation (9) is easily transformed into the standard Kelvin-Christoffel equation by applying a further Fourier transform over *z* and dividing through by ω^2 to get

$$\left[\mathbf{\Gamma}\left(\mathbf{s}_r, s_z\right) - \rho\mathbf{I}\right]\ \mathbf{u}\left(\mathbf{s}_r, s_z, \omega\right) = 0\,. \tag{10}$$

where $\mathbf{\Gamma}\left(\mathbf{s}\right) = s_z^2\mathbf{T} + \left(\mathbf{R}+\mathbf{R}^T\right)s_z + \mathbf{Q}$ is the Christoffel matrix as given in equation (5b).

One-way extrapolator

To obtain a one-way equation for elastic waves in a layered anisotropic medium, we follow the approach of Fryer and Frazer (1984, 1987), an extension of Kennett's (1983) theory. Essentially the same theory arose earlier in the field of mechanics, for time-invariant systems – elastostatics, as opposed to elastodynamics – in particular with the work of Stroh (1962), and that there has been extensive theoretical work in that field (see Ting, 1996).

As an alternative to the second order differential equation in (9), the constitutive and momentum equations in (3) can be combined into a *first-order* differential equation in *z*

$$\frac{\partial\mathbf{b}}{\partial z} = i\omega\mathbf{A}\mathbf{b}\,, \tag{11a}$$

where **b** is a vector containing displacement and the vertical components of traction – properties which are continuous across a horizontal plane – given by

$$\mathbf{b} = \begin{pmatrix} \mathbf{u} \\ \boldsymbol{\tau} \end{pmatrix}, \text{ for } \boldsymbol{\tau} = -\frac{1}{i\omega}\begin{pmatrix} \sigma_{13} & \sigma_{23} & \sigma_{33} \end{pmatrix}^T, \tag{11b}$$

and where

$$\mathbf{A} = -\begin{pmatrix} \mathbf{T}^{-1}\mathbf{R}^T & \mathbf{T}^{-1} \\ \mathbf{R}\mathbf{T}^{-1}\mathbf{R}^T - \mathbf{Q} + \rho\mathbf{I} & \mathbf{R}\mathbf{T}^{-1} \end{pmatrix}. \tag{11c}$$

In the mechanics literature, **A** is sometimes referred to as the *fundamental elasticity matrix*. Equation (11) is an eigenproblem involving a 6-by-6 system, so that there are in general six eigenvalues and eigenvectors. These have a one-to-one relationship with the three pairs of eigenvalues and corresponding paired eigenvectors which arise from the Kelvin-Christoffel equation (5). Introducing the notational convenience for vertical slowness, $q \equiv s_z \equiv s_3$, the eigendecomposition of **A** is

$$\mathbf{D}^{-1}\mathbf{A}\mathbf{D} = \boldsymbol{\Lambda} = diag\begin{pmatrix} q_P^U & q_{S1}^U & q_{S2}^U & q_P^D & q_{S1}^D & q_{S2}^D \end{pmatrix}, \tag{12}$$

where the subscripts P, S1 and S2 refer to the three modes, and the superscripts U and D distinguish between up- and down-going solutions respectively. **D** is a matrix containing the six eigenvectors of **A** as its columns.

Assuming a vertically homogeneous layer, such that **D** is independent of z, equation (12) can be substituted into (11) to give

$$\frac{\partial \mathbf{v}}{\partial z} = i\omega\boldsymbol{\Lambda}\mathbf{v}, \tag{13a}$$

where

$$\mathbf{b} = \mathbf{D}\mathbf{v} \quad \text{and} \quad \mathbf{v} = \begin{pmatrix} \mathbf{v}_U \\ \mathbf{v}_D \end{pmatrix}. \tag{13b}$$

The three elements of $\mathbf{v}_U$ are the amplitudes of up-going P, S1 and S2 waves, whilst the elements of $\mathbf{v}_D$ are the down-going amplitudes. **D** can be thought of as a composition operator which constructs the displacement-stress from the wave-mode amplitudes, whereas $\mathbf{D}^{-1}$, is a decomposition operator.

Equation (13) has the solution

$$\mathbf{v}(z) = e^{i\omega\boldsymbol{\Lambda}(z-z_0)}\mathbf{v}(z_0). \tag{14}$$

Equation (14) describes two way extrapolation in a homogeneous medium, where the solution can be split into up and down-going solutions. The separation is not straightforward in the heterogeneous case, which we now address.

Vertical heterogeneity

As is usual in wavefield extrapolation, we approximate vertical heterogeneity by a stack of homogeneous layers, each of thickness Δz, with discontinuous medium properties at interfaces between layers (Figure 4). This is a good approximation to a continuously variable medium provided the step size is not too large. The displacement-stress vector **b** is continuous across an interface. The wave-mode vector **v**, is not. One

possible approach to extrapolation would be to decompose **b** at the top interface of each layer to get **v**, extrapolate **v** within the layer using equation (14), and then recompose **b** at the lower interface where it becomes the initial wavefield for the next layer. A more economical approach is to compute the interface-propagator which extrapolates **v** infinitesimally across each interface. Based on continuity of **b** it is readily shown (e.g. Kennett, 1983) that the required interface-propagator to cross an interface at z_n, from z_n- just above the interface to z_n+ just below the interface, is simply given by

$$\mathbf{W}(z_n+, z_n-) = \mathbf{D}_n^{-1}\mathbf{D}_{n-1}, \tag{15a}$$

so that

$$\mathbf{v}(z_n+) = \mathbf{W}(z_n+, z_n-)\mathbf{v}(z_n-), \tag{15b}$$

where $\mathbf{D}_{n-1}$ is the composition matrix in layer n-1 above the interface, and $\mathbf{D}_n$ is the composition matrix in layer n, below the interface.

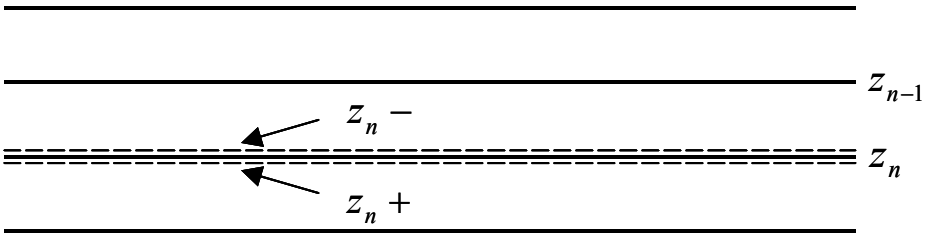

FIG. 4. Layered medium, consisting of homogenous layers with discontinuities at interfaces. Interface-propagator $\mathbf{W}(z_n+, z_n-)$ translates wavefield from above interface at z_n to just below.

Hence, all that is required to generate the interface-propagator are the matrices **D** and $\mathbf{D}^{-1}$, for each layer. Recall that the columns of **D** are the six eigenvectors

$$\mathbf{b}_i = \varepsilon_i \begin{pmatrix} \mathbf{u}_i \\ \boldsymbol{\tau}_i \end{pmatrix}, \quad i = 1,\ldots,6, \tag{16}$$

where the normalization factors ε_i are to be determined. Then, with the rows of $\mathbf{D}^{-1}$ denoted by $\mathbf{g}_i^T$, the following orthogonality relationship obviously holds:

$$\mathbf{g}_j^T \mathbf{b}_i = \delta_{ij}. \tag{17}$$

Various authors (e.g. Fryer and Frazer, 1984) have shown the simple relationship

$$\mathbf{g}_i = \mathbf{J}\mathbf{b}_i, \text{ for } \mathbf{J} \equiv \begin{pmatrix} \mathbf{0}_3 & \mathbf{I}_3 \\ \mathbf{I}_3 & \mathbf{0}_3 \end{pmatrix}, \tag{18}$$

where $\mathbf{I}_3$ and $\mathbf{0}_3$ are the 3-by-3 identity and zero matrices. Consequently, the inverse of **D** is given by

$$\mathbf{D}^{-1} = \left(\mathbf{JD}\right)^{T}. \tag{19}$$

Both $\mathbf{D}$ and $\mathbf{D}^{-1}$ are easily computed, given the eigenvectors $\mathbf{b}_i$. The top half of each $\mathbf{b}_i$, is $\mathbf{u}_i$, which is an eigenvector of the Kelvin-Christoffel equation, (5b). To obtain the stress vectors which make up the bottom half of each $\mathbf{b}_i$, we use equations (3a), (8b) and (11b) to obtain

$$\boldsymbol{\tau}_i = -(\mathbf{R} + s_z\mathbf{T})\mathbf{u}_i. \tag{20}$$

The six eigenvectors correspond to up and down-going P, S1 and S2 waves. Using the same notational convention as in equation (12), we have

$$\mathbf{D} = \begin{pmatrix} \mathbf{b}_P^U & \mathbf{b}_{S1}^U & \mathbf{b}_{S2}^U & \mathbf{b}_P^D & \mathbf{b}_{S1}^D & \mathbf{b}_{S2}^D \end{pmatrix}, \tag{21a}$$

where

$$\mathbf{b}_M^{U,D} = \varepsilon_M^{U,D}\begin{pmatrix} \mathbf{u}_M^{U,D} \\ \boldsymbol{\tau}_M^{U,D} \end{pmatrix} = \varepsilon_M^{U,D}\begin{pmatrix} \mathbf{u}_M^{U,D} \\ -\left(\mathbf{R} + q_M^{U,D}\mathbf{T}\right)\mathbf{u}_M^{U,D} \end{pmatrix}, \tag{21b}$$

$$M \in \{P, S1, S2\}.$$

Finally, the eigenvector normalization factor is given by

$$\varepsilon_M^{U,D} = \frac{1}{\sqrt{2\mathbf{u}_M^{U,D}\cdot\boldsymbol{\tau}_M^{U,D}}}. \tag{22}$$

Using this result, the interface-propagator of equation (15) is now given by

$$\begin{aligned} \mathbf{W}(z_n+, z_n-) &= \begin{pmatrix} \mathbf{g}_{P,n}^U & \mathbf{g}_{S1,n}^U & \mathbf{g}_{S2,n}^U & \mathbf{g}_{P,n}^D & \mathbf{g}_{S1,n}^D & \mathbf{g}_{S2,n}^D \end{pmatrix}^T \\ &\times \begin{pmatrix} \mathbf{b}_{P,(n-1)}^U & \mathbf{b}_{S1,(n-1)}^U & \mathbf{b}_{S2,(n-1)}^U & \mathbf{b}_{P,(n-1)}^D & \mathbf{b}_{S1,(n-1)}^D & \mathbf{b}_{S2,(n-1)}^D \end{pmatrix}, \\ &= \begin{pmatrix} \mathbf{W}_{UU}(z_n+, z_n-) & \mathbf{W}_{UD}(z_n+, z_n-) \\ \mathbf{W}_{DU}(z_n+, z_n-) & \mathbf{W}_{DD}(z_n+, z_n-) \end{pmatrix} \end{aligned} \tag{23}$$

where

$$\mathbf{W}_{KL}(z_n+, z_n-) = \begin{pmatrix} \mathbf{g}_{P,n}^K\cdot\mathbf{b}_{P,(n-1)}^L & \mathbf{g}_{P,n}^K\cdot\mathbf{b}_{S1,(n-1)}^L & \mathbf{g}_{P,n}^K\cdot\mathbf{b}_{S2,(n-1)}^L \\ \mathbf{g}_{S1,n}^K\cdot\mathbf{b}_{P,(n-1)}^L & \mathbf{g}_{S1,n}^K\cdot\mathbf{b}_{S1,(n-1)}^L & \mathbf{g}_{S1,n}^K\cdot\mathbf{b}_{S2,(n-1)}^L \\ \mathbf{g}_{S2,n}^K\cdot\mathbf{b}_{P,(n-1)}^L & \mathbf{g}_{S2,n}^K\cdot\mathbf{b}_{S1,(n-1)}^L & \mathbf{g}_{S2,n}^K\cdot\mathbf{b}_{S2,(n-1)}^L \end{pmatrix}, \tag{24}$$

$$K, L \in \{U, D\}.$$

Note that if there is no contrast in properties across the interface, both layers have the same eigenvectors, and the orthogonality property (17) comes into play, so that $\mathbf{W}$ is the identity matrix. Equation (24) describes four 3-by-3 matrices corresponding to the

combinations of up and down-going waves in layers (n-1) and n. For the purposes of one-way extrapolation, we will be interested in $\mathbf{W}_{DD}$ for the source side and $\mathbf{W}_{UU}$ for the receiver side, consistent with the assumption that backscattered energy can be ignored.

To clarify this, consider the wave-mode vector **v** either side of the interface:

$$\mathbf{v}(z_n+) = \mathbf{W}(z_n+, z_n-)\mathbf{v}(z_n-). \tag{25}$$

Now assume that there is *no* up-going wave so that, at both z_n- and z_n+ we have

$$\mathbf{v}(z) = \begin{pmatrix} \mathbf{0} \\ \mathbf{v}_D(z) \end{pmatrix}. \tag{26}$$

where **0** is the 3-vector of zero values. Substitution into (25) then gives

$$\mathbf{v}_D(z_n+) = \mathbf{W}_{DD}(z_n+, z_n-)\mathbf{v}_D(z_n-). \tag{27}$$

Now, defining $\mathbf{\Lambda}_D = diag\begin{pmatrix} q_P^D & q_{S1}^D & q_{S2}^D \end{pmatrix}$, and using equation (14), the complete extrapolation from the bottom of layer (n-1) to the bottom of layer n, can be written

$$\mathbf{v}_D(z_n+) = \mathbf{W}_{DD}(z_n+, z_n-)e^{i\omega\mathbf{\Lambda}_D(z_n - z_{n-1})}\mathbf{v}_D(z_{n-1}+) \tag{28}$$

The one-way decomposition and composition relationships are given by

$$\mathbf{v}_D = \mathbf{D}_D^{-1}\mathbf{b}, \tag{29a}$$

and

$$\mathbf{b}_D = \mathbf{D}_D\mathbf{v}_D, \tag{29b}$$

where $\mathbf{D}_D = \begin{pmatrix} \mathbf{b}_P^D & \mathbf{b}_{S1}^D & \mathbf{b}_{S2}^D \end{pmatrix}$ is the 6-by-3 matrix which generates the displacement-stress vector associated with only down-going P, S1 and S2 waves, and $\mathbf{D}_D^{-1} = \begin{pmatrix} \mathbf{g}_P^D & \mathbf{g}_{S1}^D & \mathbf{g}_{S2}^D \end{pmatrix}^T$ is the 3-by-6 matrix which takes a displacement-stress vector and extracts the down-going wave-modes. Incidentally, substitution of (29a) into (29b) shows that the matrix $\mathbf{D}_D\mathbf{D}_D^{-1}$ is a *projection* of **b** onto its down-going part $\mathbf{b}_D$.

The combination of equation (29a) applied at an initial depth, recursive application of equation (28), and the use of equation (29b) at a final depth, describes forward extrapolation of the down-going elastic wavefield. Similar equations involving $\mathbf{W}_{UU}(z_n-, z_n+)$ describe backward extrapolation of the up-going wavefield.

Figure 5 shows graphically interface-propagators for an interface between two isotropic media with a P-wave velocity change from 2800m/s to 3200m/s, and an S-wave velocity change from 1400m/s to 1600m/s. The propagators are shown for P-wave angles of (a) 0° and (b) 60°. Figure 6 shows the same for an isotropic medium over an HTI medium with an axis of symmetry at 45° azimuth. Salient points are: (i) that there are no off-diagonal terms for isotropic contrasts at vertical incidence, since there are no mode conversions, but at non-zero angles of incidence there are off-diagonal terms corresponding to conversion between P and SV modes; and (ii) for the HTI case there is

strong normal incidence conversion to S1 and S2 modes from SV or SH modes, corresponding to shear-wave splitting, described by a rotation matrix with 45° azimuth. This also occurs at non-zero angles, but is asymmetric, such that a simple rotation matrix based on 45° azimuth is no longer valid (Figure 6(b)).

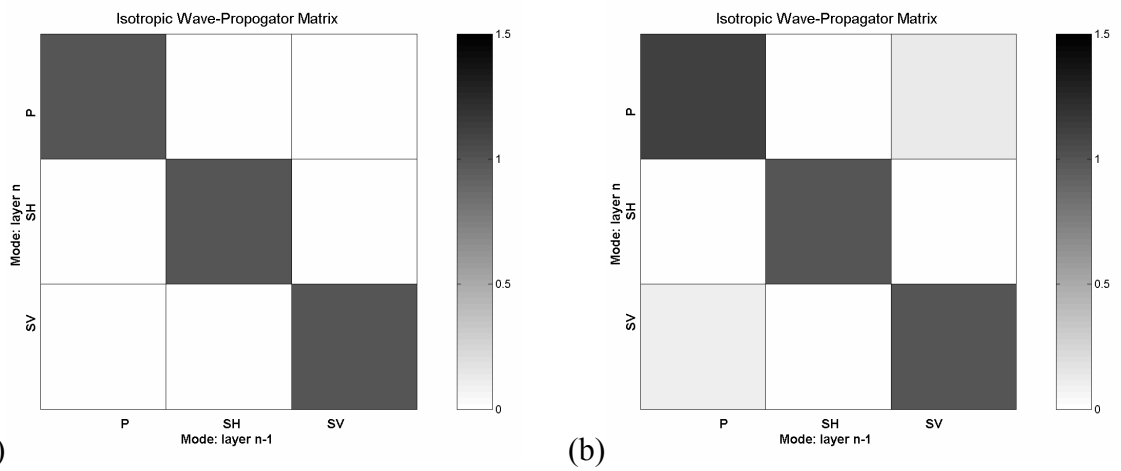

(a) (b)

FIG. 5. Interface-propagator matrices for isotropic medium contrast, from layer n-1 (v_P=2800m/s, v_S=1400m/s) to layer n (v_P=3200m/s, v_S=1600m/s). P-wave incidence angles are (a) 0° and (b) 60°.

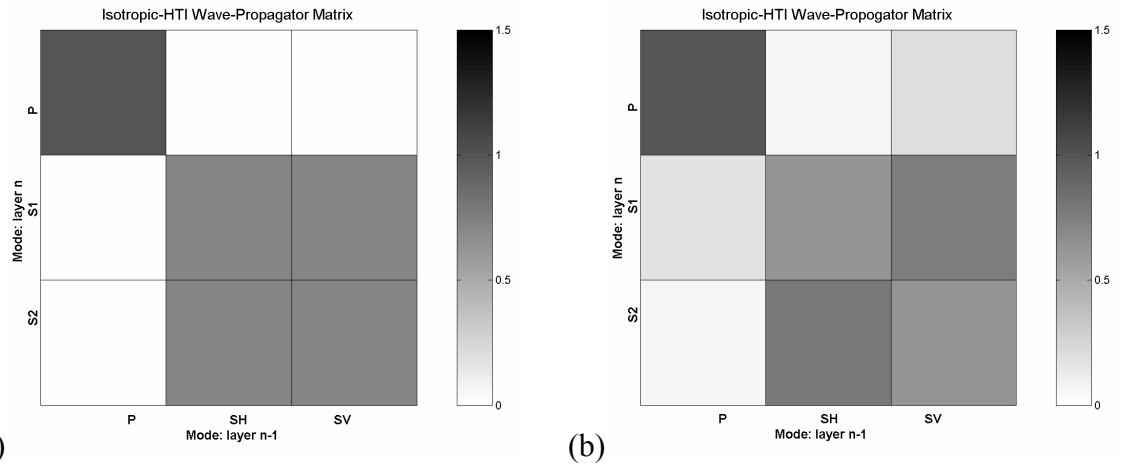

(a) (b)

FIG. 6. Interface-propagator matrices for isotropic (layer n-1) to HTI (layer n) medium contrast. P-wave incidence angles are (a) 0° and (b) 60°. The axis of symmetry for the second medium is at 45° azimuth.

The formulation of the extrapolator in terms of interface-propagators, as in equation (28), is more efficient than explicit mappings between **v** and **b** at each interface, but also affords another advantage. Since the one-way interface-propagators $\mathbf{W}_{DD}$ and $\mathbf{W}_{UU}$ are 3-by-3 matrices which describe the conversion between modes across interfaces, we can choose to be selective about which mode conversions are honoured when extrapolating the wavefield. Doing so can reduce sensitivity to errors in the model, and so prevent the generation of spurious artifacts. The same approach was taken by Silawongsawat (1998) in the context of forward modelling, as an aid to interpretation of the modelled results. The simplest approximation is to use only the diagonal elements of the interface-

propagators, which corresponds to ignoring all mode conversions during extrapolation. In this case the algorithm reduces to pure scalar extrapolation, as in equation (14).

Boundary conditions

In order to commence downward extrapolation, we first need either a displacement-stress vector, $\mathbf{b}(z_0)$, or the wave-mode vector $\mathbf{v}(z_0)$ in the top layer. Since generally only displacement (or velocity, the time derivative of displacement) is measured, there remains the problem of determining the stress vector, or alternatively the wave-modes directly. We consider two scenarios and show how this problem is resolved in each case, without additional measurements.

Free surface boundary condition

The simplest case is when the wavefield is recorded on a free surface, such as the earth-air interface. A free surface has zero stress, which is easily incorporated into the vector $\mathbf{b}(z_0)$, which simply becomes:

$$\mathbf{b}(z_0) = \begin{pmatrix} \mathbf{u}(z_0) \\ \mathbf{0} \end{pmatrix}, \tag{30}$$

where $\mathbf{0}$ is the 3-vector of zero values. This can then be substituted into (29a) to obtain the down-going wave-mode vector, $\mathbf{v}_D(z_0)$. This is then used to initiate the recursion of equation (28).

One-way boundary condition

A second possible scenario assumes that up-down separation has been applied, so that we can assume waves propagating in only the down-going direction (or up-going, if at the receiver side). In this case we have a wave-mode vector of the following form:

$$\mathbf{v}(z_0) = \begin{pmatrix} \mathbf{0} \\ \mathbf{v}_D(z_0) \end{pmatrix}. \tag{31}$$

From equation (29b), we can deduce:

$$\mathbf{u}(z_0) = \mathbf{D}'_D \mathbf{v}_D(z_0), \tag{32}$$

where $\mathbf{D}'_D = \begin{pmatrix} \mathbf{u}_P^D & \mathbf{u}_{S1}^D & \mathbf{u}_{S2}^D \end{pmatrix}$ is the 3-by-3 matrix containing the first 3 rows of $\mathbf{D}_D$.

Inverting equation (32) we get:

$$\mathbf{v}_D(z_0) = \left[\mathbf{D}'_D\right]^{-1} \mathbf{u}(z_0). \tag{33}$$

In this case, the algorithm commences with equation (33), which then initiates the recursive extrapolation of equation (28).

The down-going cases described here are relevant for the shot side. Similar equations obtain for the up-going waves in both cases, as is required on the receiver side.

NUMERICAL EXAMPLES

Homogeneous isotropic medium

The first example we present to illustrate the algorithm is wavefield extrapolation in a homogeneous isotropic medium. The P and S velocities are 3000m/s and 1500m/s respectively. Figure 7 demonstrates the operator construction by way of an impulse response for a 200m *downward* extrapolation of the *up-going* wavefield. The "impulse" is a bandlimited spike on the u_z component (a). After the decomposition step (here assuming a free surface condition), the P and SV (labelled S2 in figures) inputs, $v_P(z_0)$ and $v_{SV}(z_0)$, are shown in (b). Since this is isotropic, there is no SH response. The extrapolated P and SV modes, $v_P(z_1 = z_0 + 200m)$ and $v_{SV}(z_1)$, are shown in (c). Finally the displacements at the new depth, $u_x^U(z_1)$ and $u_z^U(z_1)$, are shown in (d). During extrapolation, we have used add a small (1%) imaginary velocity to the true velocity in order to both stabilize the decomposition by avoiding singularities and to suppress Fourier wrap around artifacts.

Figure 8 shows the FK amplitude spectra of the extrapolated result as in Figure 7(d), though in this case we only used 0.01% imaginary velocity, in order to better see the full FK response. In the FK domain, the relationship between propagating and evanescent areas is easily seen, with an interference effect occurring where both P- and S-modes are propagating.

In Figure 9 the output from Figure 7 is extrapolated back upwards to the original depth. The residual energy on the X component arises because the P-wave evanescent area between the maximum P- and SV-wave slownesses cannot be recovered.

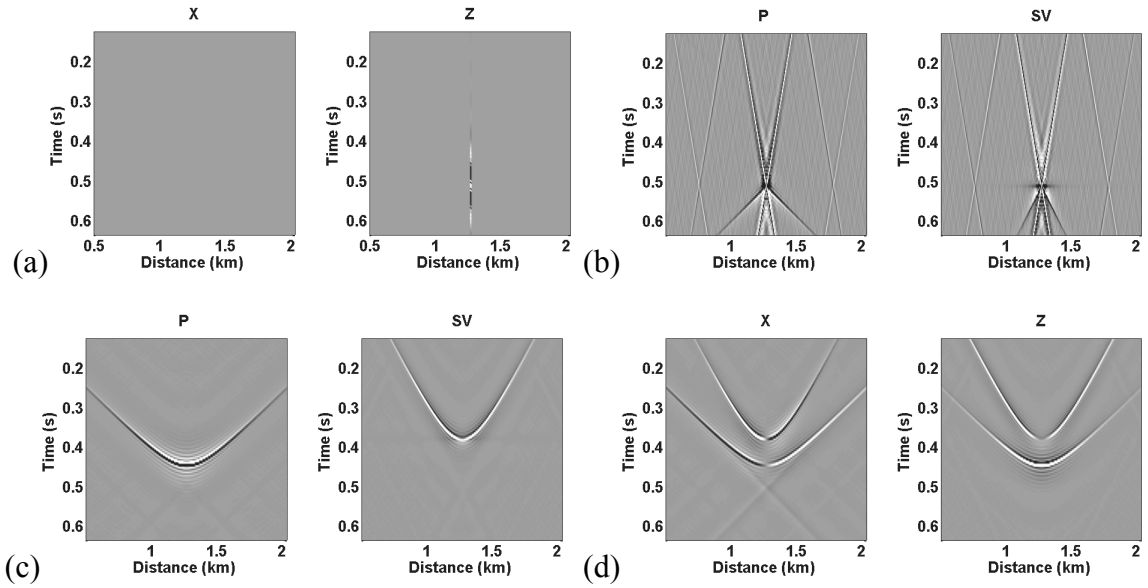

FIG. 7. Wavefield extrapolator impulse response construction for homogeneous, isotropic medium: (a) input bandlimited spike on z component; (b) after decomposition into up-going P and SV (S2) modes; (c) after extrapolation downward by 200m; (d) after recomposition to X and Z components. Plots have the same display scaling applied.

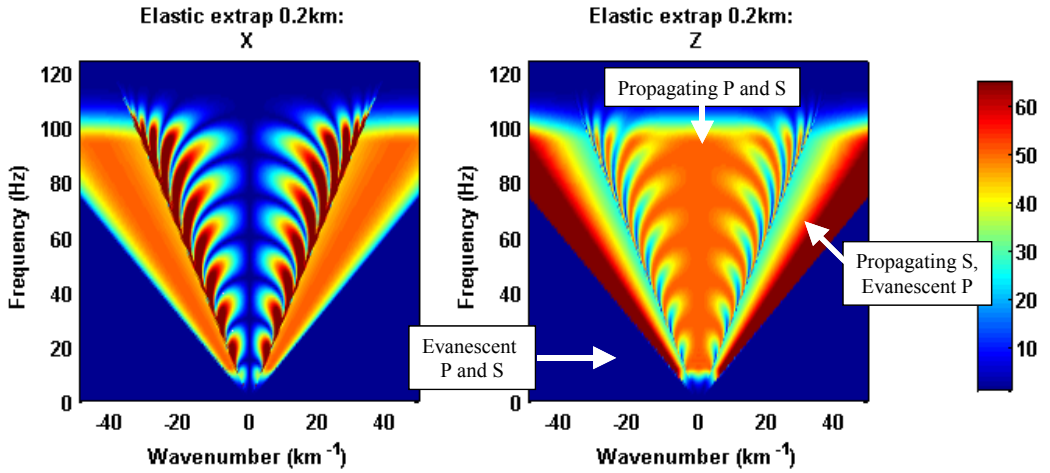

FIG. 8. FK spectra of extrapolated displacements, as in Figure 7(d) but using only 0.01% imaginary velocity.

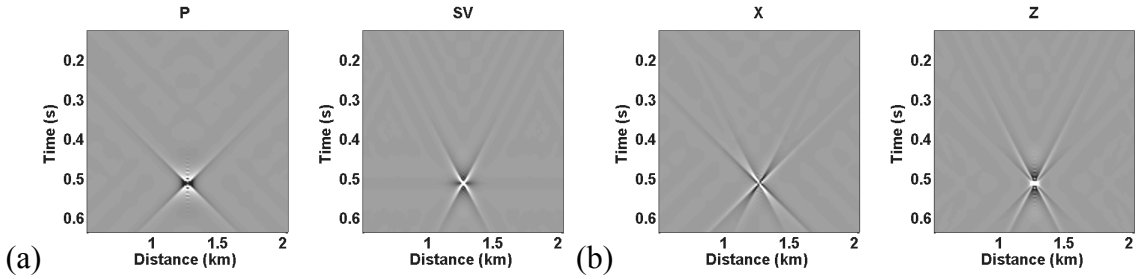

FIG. 9. Result of applying inverse extrapolation operator to impulse response shown in Figure 7: (a) upward extrapolated P and SV modes; (b) after recomposition to X and Z components. Compare (a) with Figure 7(b) and (b) with Figure 7(a). Plots have the same display scaling applied as in Figure 7.

Homogeneous HTI medium

In Figure 10, the operator in an HTI medium is illustrated by way of impulse responses, using the same input as for the isotropic example in Figure 7. Two examples are shown: one, (a), for an axis of symmetry aligned with the x direction; and another, (b), for an axis of symmetry at 45° azimuth to the x axis. Only the extrapolated wave-modes are shown in both cases. The anisotropy gives rise to triplications along the plane which contains the symmetry axis, as can be seen in (a), and to an S2 response in the case where the symmetry axis is rotated as is seen in (b).

We now apply the wavefield extrapolation to modelled data, in a homogeneous HTI medium. The modelled data are generated using the pseudospectral method (Bale, 2002a, 2002b), for an HTI medium with an axis of symmetry at 45° azimuth to the x axis. The geometry for the modelling is shown in Figure 11. The source is a vertical displacement force at 1000 m depth. An absorbing boundary is placed along all four edges of the domain, so that only up-going waves are recorded, apart from some low level residual reflection due to imperfect absorption. We record the wavefield at three different levels, A, B, and C, as shown in Figure 11. This allows direct comparison of the data extrapolated from A to B or C, with the true data at those depths.

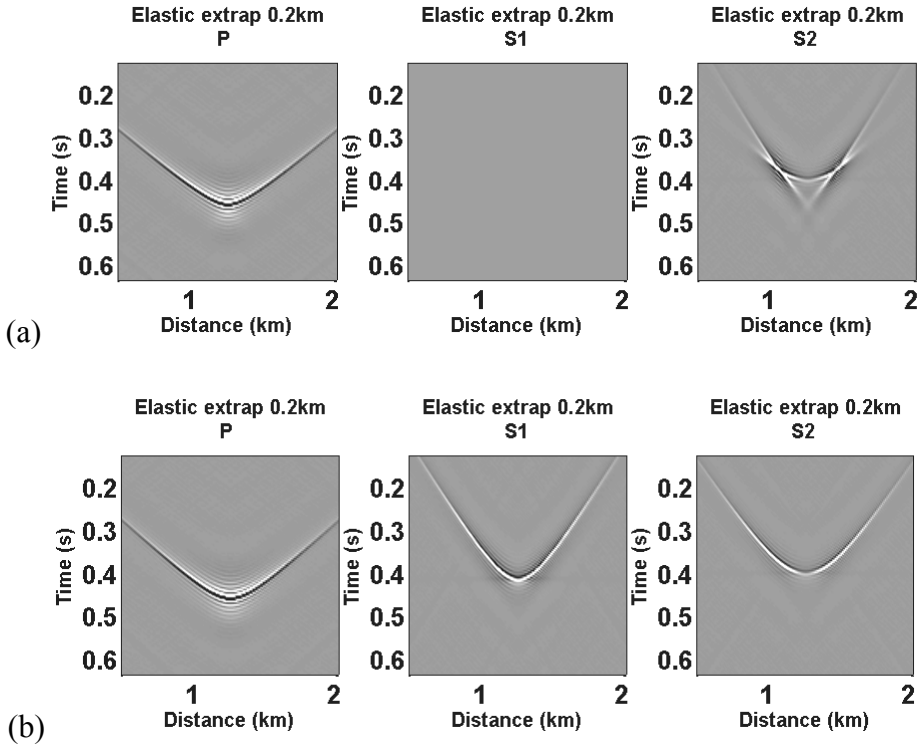

FIG. 10. A comparison of impulse responses for HTI media with different symmetry axes. The wave-modes prior to recomposition are shown, for the same impulse input as in Figure 7, after extrapolation 200m downwards in an HTI medium: (a) with axis of symmetry along the x direction; (b) with axis of symmetry at 45° azimuth to the x direction. Note the presence of triplications for the SV (S2) mode when the plane contains the symmetry axis.

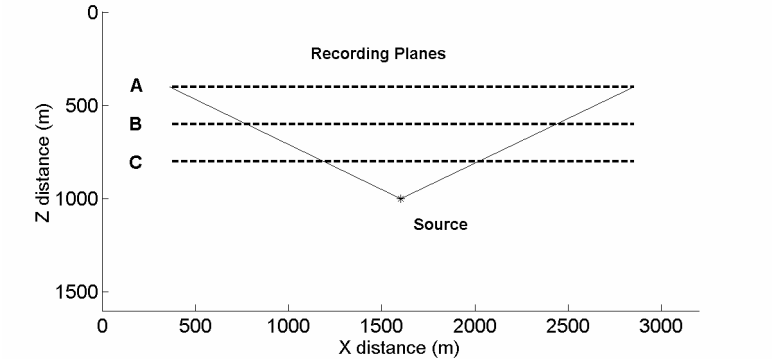

FIG. 11. Geometry of modelled data. Vertical displacement source generates P- and S-waves at depth of 1000m, these are recorded at three different levels shown by dashed lines: A (400m), B (600m) and C (800m). Solid diagonal lines show angular aperture limitation during extrapolation.

Figure 12 shows the result of downward extrapolating the data from level A to level B. The input data are shown in (a). The extrapolation is broken down into the following steps: (b) decomposition into wave-modes, P, S1 and S2, at A; (c) extrapolation and recomposition at B. Compare the result in (c) with the modelled wavefield at level B, shown in (d). The differences are primarily the result of aperture limitations, since the angular aperture at A is smaller than that at B, for the same width of recording array. This effect comes into play during downward (backward) extrapolation of the receivers in shot migration, and is inherent in the geometry.

By contrast, consider Figure 13, which shows the upward extrapolation of the wavefield from level C, (a), to levels B, (b) and A, (c). As can be seen by comparison with the modelled results in Figure 11, extrapolation gives accurate results in this direction. This is because the angular aperture of the input wavefield is broader than that of either outputs. This geometry (with the Z axis inverted) is relevant to downward (forward) extrapolation of a shot. The results in Figures 12 and 13 confirm that the elastic wavefield extrapolation is working as intended for an HTI medium.

Vertically heterogeneous HTI medium

The final example illustrates the effect of vertical heterogeneity on the extrapolation. The model used, as shown in Figure 14, consists of two layers: an isotropic layer overlying the same HTI layer as used in the previous example.

Figure 15 shows the results of extrapolating input at level C by 400m upwards to level A: (a) using the full matrix for the one-way interface-propagator across the interface, corresponding to all transmission conversions; (b) including only diagonal terms of the matrix, corresponding to neglecting all conversions; and, (c) excluding the P-to-S conversions but including the S1 to S2 conversions. The weaker, flatter events are spurious reflections from the model boundary and should be ignored. The result from using the full matrix, in (a), compares well with the modelled data in (d), even recovering the weak P-to-S conversion visible after the first arrival on the X-component. While ignoring the P-to-S conversions has a small impact on the extrapolated data (compare (c) with (a), and with (d)), it is evident that ignoring all conversions, (b), is inadequate in this example. To do so ignores the rotation of the anisotropy symmetry axis. Including the S1-S2 conversion terms in the interface-propagator matrix essentially embeds a generalized Alford rotation within the extrapolation, and is a necessary step when imaging in the presence of azimuthal anisotropy.

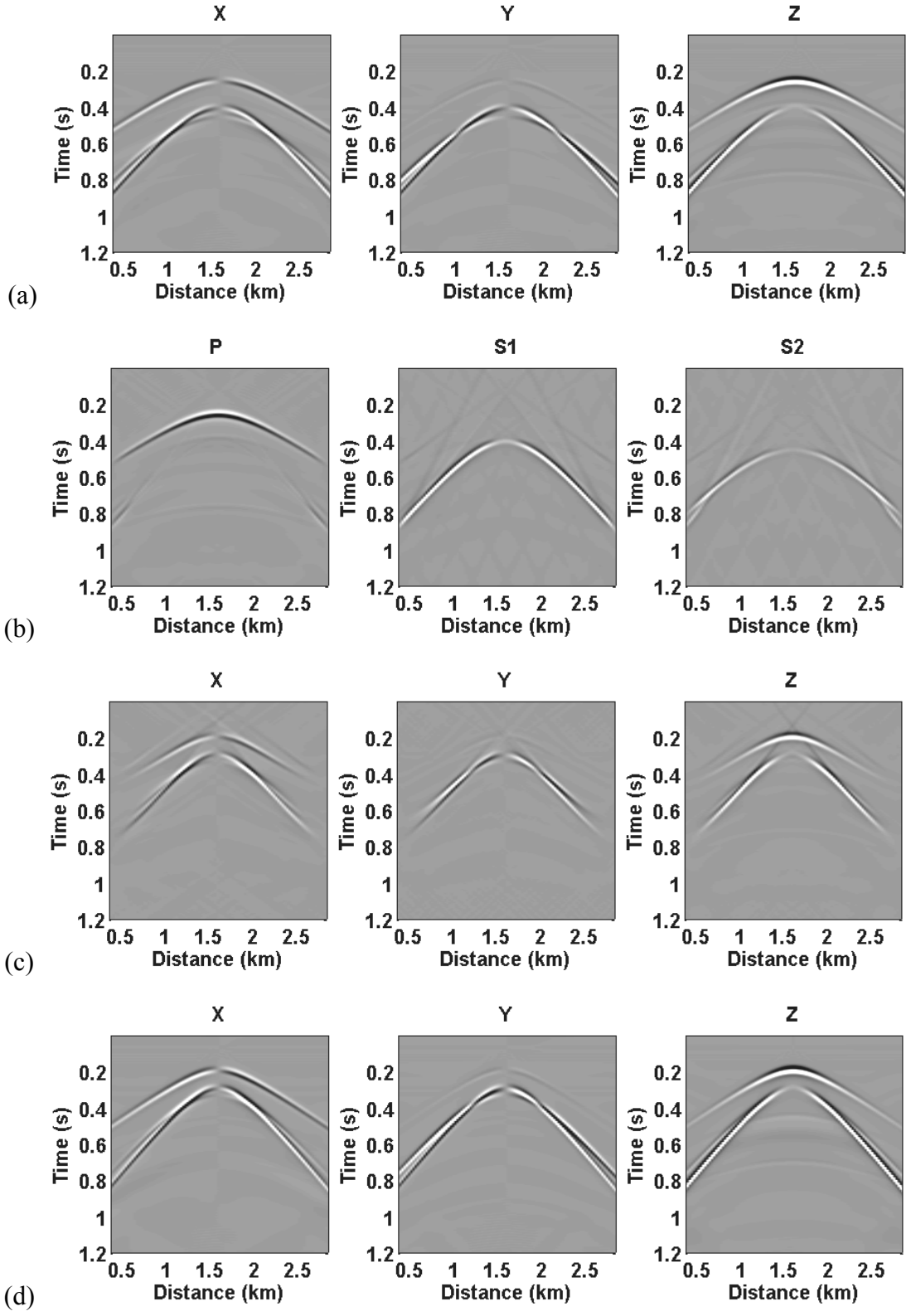

FIG. 12. Downward extrapolation of modelled HTI data: (a) displacement wavefield recorded at A (see Figure 10); (b) after wavefield decomposition into P, S1 and S2 modes; (c) after extrapolation and recomposition to displacement at B; (d) data recorded at B from forward modelling. Compare the result of extrapolation, (c), with modelled data at B, (d).

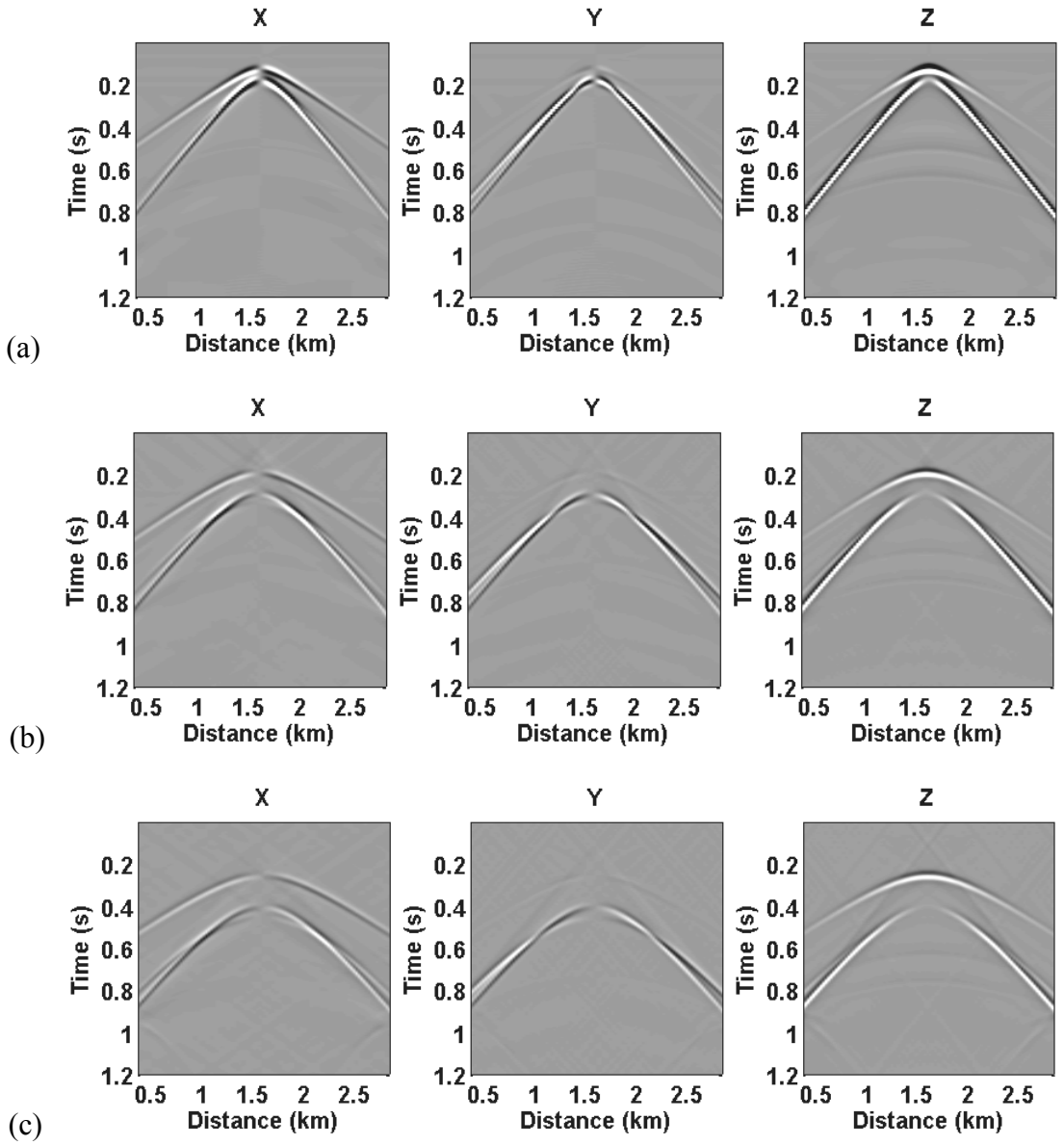

FIG. 13. Upward extrapolation of modelled HTI data: (a) displacement wavefield recorded at C (see Figure 10); (b) extrapolated upwards to B - compare with Figure 11(d); (c) extrapolated upwards to A – compare with Figure 11(a).

CONCLUSIONS

The extrapolation of elastic waves consists of first decomposing the displacement wavefield into wave-modes P, S1 and S2, using an appropriate boundary condition assumption, and then recursive application of phase-shift operators and an "interface-propagator" matrix operation which handles the effects of medium changes at each depth interface. This is equivalent to reconstructing the displacement-stress vector which is continuous across each interface. The operators which achieve this are found by solving the Kelvin-Christoffel equation. The eigenvalues of the Kelvin-Christoffel equation lead

directly to the phase-shift operators, whilst the eigenvectors give the polarizations of displacement. The relationship between stress and displacement is then used to compute eigenvectors of the appropriate one-way equation, and from these we determine the interface-propagators. The solution to the Kelvin-Christoffel equation is analytic for the HTI case, and the up- and down-going solutions are also simply related in this case. The choice of whether to use down-going or up-going solutions depends on whether we are forward extrapolating a downward-propagating source wavefield, or backward extrapolating an upward-propagating receiver wavefield.

The structure of the interface-propagator matrices allows the selective inclusion of forward-scattered mode-conversions in the extrapolator. This allows neglect of conversions which might become generators of spurious noise, due to model inaccuracies. In particular we suggest that in general P-to-S conversion may be safely neglected (except, of course, for conversion on reflection, which would be dealt with in migration by an appropriate imaging condition). However, in the case of the interface between an isotropic and an HTI medium, we find that inclusion of the S1-S2 conversions is important to proper extrapolation of the wavefield. It is therefore expected that this form of extrapolator will be useful in imaging fractured media where shear-wave splitting is a significant factor. Use of this kind of extrapolator could be regarded as a form of generalized Alford rotation, which is not limited by assumptions of dip or offset.

ACKNOWLEDGEMENTS

The authors would like to acknowledge the support of sponsors of the CREWES project and of the POTSI project, towards this work.

The authors also thank Steve Horne of WesternGeco for helpful discussions related to this work, and also Ed Krebes and Jeff Grossman of University of Calgary, for their careful reviews and comments.

REFERENCES

Aki, K. and Richards, P.G., 1980, Quantitative Seismology: Theory and Methods, Vol.1: New York, W.H. Freeman and Co.

Alford, R.M., 1986, Shear data in the presence of azimuthal anisotropy: Dilley, Texas: 56th Ann. Internat. Mtg., Soc. Expl. Geophys., Expanded Abstracts, 476–479.

Bale, R.A., 2002a, Modelling 3D anisotropic elastic data using the pseudospectral approach: CREWES Research Report, **14.**

Bale, R.A., 2002b, Staggered grids for 3D pseudospectral modelling in anisotropic elastic media: CREWES Research Report, **14**

Bale, R., Dumitru, G, and Probert, T., 2000, Analysis and stacking of 3-D converted-wave data in the presence of azimuthal anisotropy: 70th Annual Internat. Mtg. Soc. Expl. Geoph., Expanded Abstracts, 1189-1192.

Bale, R.A. and Margrave, G.F., 2003, Adapting elastic wavefield extrapolation to laterally varying HTI media: CREWES Research Report, Vol. **15**, this volume.

Dellinger, J., and Etgen, J., 1990, Wave-field separation in two-dimensional anisotropic media: Geophysics, **55**, 914–919.

Etgen, J.T., 1988, Prestacked migration of P and Sv-waves, 58th Ann. Internat. Mtg: Soc. of Expl. Geophys., Session: S12.4.

Fryer, G.J. and Frazer, L.N., 1984, Seismic waves in stratified anisotropic media: Geophys. J. Roy. Astr. Soc., **78**, 691-710.

Fryer, G.J. and Frazer, L.N., 1987, Seismic waves in stratified anisotropic media—II. Elastodynamic eigensolutions for some anisotropic systems: Geophys. J. Roy. Astr. Soc., **91**, 73–101.
Gaiser, J., 2000, Advantages of 3-D P-S-wave data to unravel S-wave birefringence for fracture detection, 70th Ann. Internat. Mtg: Soc. of Expl. Geophys., 1201-1204.
Gazdag, J., 1978, Wave equation migration with the phase-shift method: Geophysics, **43**., 1342-1351.
Gazdag, J. and Sguazerro, P., 1984, Migration of seismic data by phase shift plus interpolation: Geophysics, **49**, 124 - 131.
Grossman, J.P., Margrave, G.F., and Lamoureux, M.P., 2002a, Fast wavefield extrapolation by phase-shift in the nonuniform Gabor domain: CREWES Research Report, **14**.
Grossman, J.P., Margrave, G.F., and Lamoureux, M.P., 2002b, Constructing adaptive nonuniform Gabor frames from partitions of unity: CREWES Research Report, **14.**
Hou A. and Marfurt, K., 2002, Multicomponent prestack depth migration by scalar wavefield extrapolation: Geophysics, **67**, 1886-1894.
Kennett, B.L.N., 1983, Seismic Wave Propagation in Stratified Media, Cambridge University Press.
Margrave, G.F. and Ferguson, R.J., 1999, Wavefield extrapolation by nonstationary phase shift: Geophysics, **64**, 1067-1078.
Musgrave, M.J.P., 1970, Crystal Acoustics: Introduction to the Study of Elastic Waves and Vibrations in Crystals, Holden-Day.
Shuvalov, A.L., 2001, On the theory of plane inhomogeneous waves in anisotropic elastic media: Wave Motion, **34** (4), 401-429.
Silawongsawat, C., 1998, Elastic Wavefield Modeling by Phase Shift Cascade, M.Sc. Thesis, Univ. of Calgary.
Stoffa, P.L., Fokkema, J.T., de Luna Freire, R.M., and Kessinger, W.P., 1990, Split-step Fourier migration: Geophysics, **55**, 410–421.
Stroh, A.N., 1962, Steady state problems in anisotropic elasticity, J. Math. Phys. **41**, 77-103.
Ting, T.C.T., 1996, Anisotropic Elasticity: Theory and Applications, Oxford University Press.
Wapenaar, C. P. A., and Berkhout, A. J., 1989, Elastic wave field extrapolation: Redatuming of Single- and Multi-component Seismic Data, Elsevier Science Publ. Co., Inc.
Zhe, J., and Greenhalgh, S. A., 1997, Prestack multicomponent migration: Geophysics, **62**, 590–613.

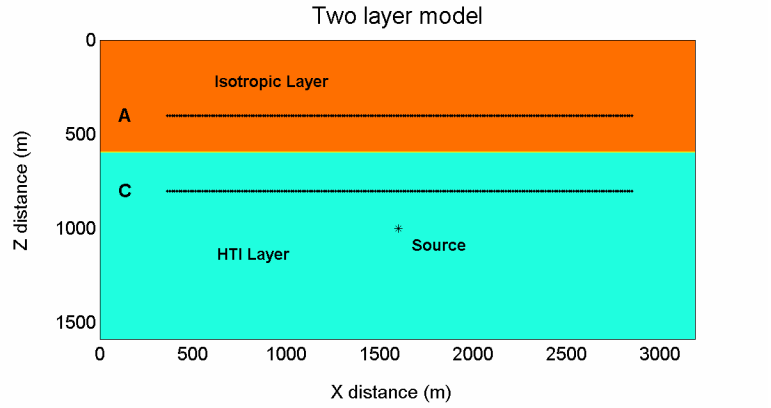

FIG. 14. Two-layer model consisting of an isotropic medium overlaying an HTI medium with axis of symmetry at 45° azimuth. Modelled data generated at levels A and C, located as before.

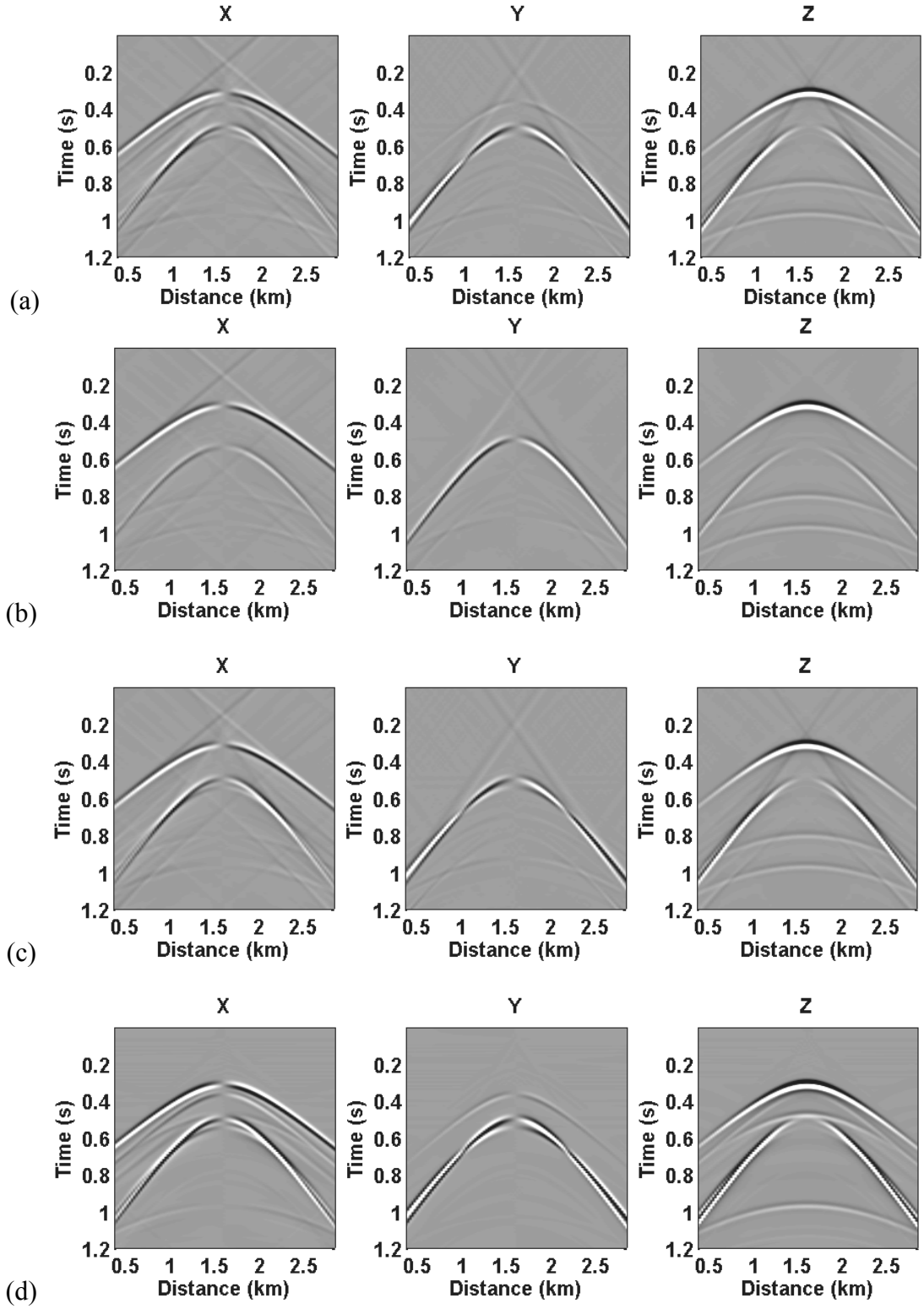

FIG. 15. Upward extrapolation, from C to A, through two layer model of Figure 14: (a) extrapolation using full one-way interface-propagator matrices across boundary, including all mode conversions; (b) extrapolation using only diagonal matrices, neglecting all conversions; (c) extrapolation using matrix with P-S conversions neglected; (d) modeled data at level A.